LA-8930-MS

Los Alamos National Laboratory is operated by the University of California for the United States Department of Energy under contract W-7405-ENG-36.

Computer Modeling of an All-Secondary Explosive Hot-Wire Device

Los Alamos National Laboratory
Los Alamos, New Mexico 87545

LA-8930-MS

UC-45
Issued: August 1981

Computer Modeling of an All-Secondary Explosive Hot-Wire Device

Daniel T. Varley III

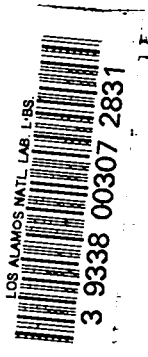

COMPUTER MODELING OF AN ALL-SECONDARY EXPLOSIVE HOT-WIRE DEVICE

by

Daniel T. Varley III

ABSTRACT

This report describes a computer model of an all-secondary explosive hot-wire device. The model accounts for the ignition of the explosive by electrical heating of a wire and the shearing of a flying plate that is subsequently used to detonate a second explosive. The results obtained from the model are in excellent agreement with experimental data.

I. INTRODUCTION

In the past three years, the Los Alamos National Laboratory has been engaged in the development of all-secondary explosive hot-wire devices. During this time, extensive experimentation was conducted to identify and examine the important parameters involved. Inquiries and literature searches indicated that most hot-wire devices were developed in just this way.

It is obvious that a numerical model of any process or processes in an electroexplosive device would facilitate greatly the design of these devices because parameters can be optimized with a minimum of experimentation. In addition, the effect of production variations on performance could be evaluated before parts are manufactured.

This report describes the modeling of two processes in a hot-wire detonator. The first is the igniting of the explosive by an electrically heated bridge and the second is the shearing of a flying plate by the pressure produced from the burning explosive. These two aspects were addressed in the onset of the modeling effort because of the ease with which existing computer codes could be adapted.

The hot-wire ignition process is common to all electroexplosive devices that use an electrically heated bridge to ignite an explosive material. The model includes both round wire and thin, flat bridges. The electric current can be input in the form of a sinusoid, ramp, or constant-magnitude function. When the temperature of the bridge material reaches the melt temperature, electrical heat generation ceases. Any explosive material can be modeled if coefficients are available for a first-order Arrhenius rate equation.

After the explosive is ignited, pressure is generated as the explosive burns. At some pressure level, the flying plate shears and attains a velocity proportional to the driving pressure. The size, mass, and velocity of the flying plate determine whether the plate will detonate an explosive upon impact. In addition, the pressure when the plate shears determines how strong the confining body of the hot-wire detonator needs to be.

II. THE EXPERIMENTAL DATA

Some experimental data are available that pertain to the two processes that were modeled. These data were used to judge the accuracy of the computed results in a circuitous fashion because the quantities that were calculated could not be measured.

In the case of explosive ignition, the experimental data consist of measured function times and firing current thresholds for several wire diameters. The function times were measured at an environmental temperature of -54°C with a time interval counter. The function time includes the igniting of HMX* explosive by a hot-wire, the burning of the explosive, the shearing of a flying plate, and the closing of a switch by the flying plate after 7.0 mm of travel. The numerical model calculated only the time to ignition at a given current level. Thus, the function time that was measured at four current levels should be larger than any calculated time to ignition. However, because the burning of the explosive takes only fractions of a millisecond and the time for the plate to travel the 7.0 mm is about 14 μs, most of the function time is the ignition time.

The function time data can also be used in another form. At a given environmental temperature, the burn time of the explosive, the shearing of the plate, and the velocity of the flying plate should be constant. This implies

*1,3,5,7 - Tetranitro - 1,3,5,7 - Tetrazacyclooctane

that the differences in the function times are due to a change in the time to ignition caused by a change in firing current. This is not strictly true because a high firing current would light the explosive promptly, whereas a low current would cause the explosive to cook before ignition and then take longer to build up to a rapid burn.

The firing current threshold and standard deviation for each wire diameter were obtained by firing 10 or more detonators in a Bruceton sensitivity test. Each detonator was deemed to have fired, or ignited, if the flying plate sheared at the test current level. The results are shown in Fig. 1 for six wire diameters. The error bars indicate one standard deviation above and below the threshold point.

At the time this report was written, no data were available on the pressure at which the flying plate sheared loose. Also, there had not been any reliable velocity measurements made from which a pressure could be determined. The only data available for estimating a plate velocity were from detonations produced in explosive pellets by flying plates. An aluminum flying plate that is 0.75 mm thick and 2.5 mm in diameter will cause detonation in PETN* explosive at a density of 1.6 g/cm^3, but will not detonate HNS** explosive at 1.55 g/cm^3. The critical energy required for impact initiation of PETN at this density is about 4 cal/cm^2.[1] For the size of the flying plate tested, a minimum velocity of 0.5 mm/μs would be necessary. HNS explosive has a critical energy of 34 cal/cm^2, and a velocity of 1.4 mm/μs would be needed for detonation.

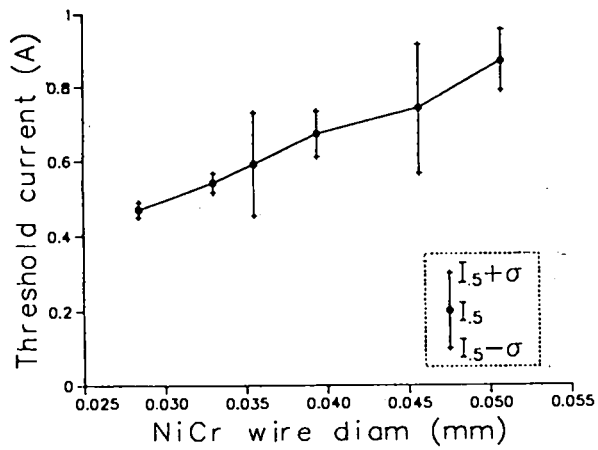

Fig. 1
Threshold as a function of wire diameter.

*Pentaerythritol Tetranitrate
**2,2',4,4',6,6' - Hexanitrostilbene

III. THE EXPERIMENTAL DEVICE

Figure 2 shows a drawing of the ER-322 flying plate detonator that was used to obtain the experimental data. The steel header in this hot-wire device contains a compression glass substrate with two independent and welded bridgewires. In the standard assembly, each bridgewire was 0.051-mm-diam Tophet C, and the assembly resistance was nominally 0.88 ohms through each bridgewire and electrode. Figure 3 shows a photographic enlargement of the bridgewire area.

HMX explosive is loaded against the bridgewires to a density of 1.67 g/cm^3. The detonator contains 0.10 g of HMX, and the specific surface of the HMX is 8300 cm^2/g.

To obtain the confinement needed for hot-wire initiation of HMX, a 0.75-mm-thick 6061-T6 aluminum closure plate was used.[2] The barrel assembly is screwed on to hold the closure disk in place. The barrel is 2.5 mm in diameter and 7.0 mm long, and the center of the closure plate shears into the barrel to form the flying plate.

The function times and the initiation of PETN and HNS were determined using the standard assembly shown in Fig. 2. In the threshold testing, only the diameter of the bridgewire was changed.

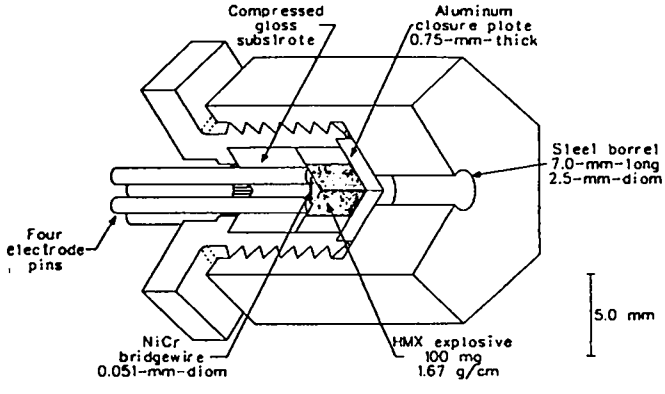

Fig. 2
The ER-322 all-HMX explosive hot-wire flying-plate detonator. Only one of two independent bridgewires is shown for clarity.

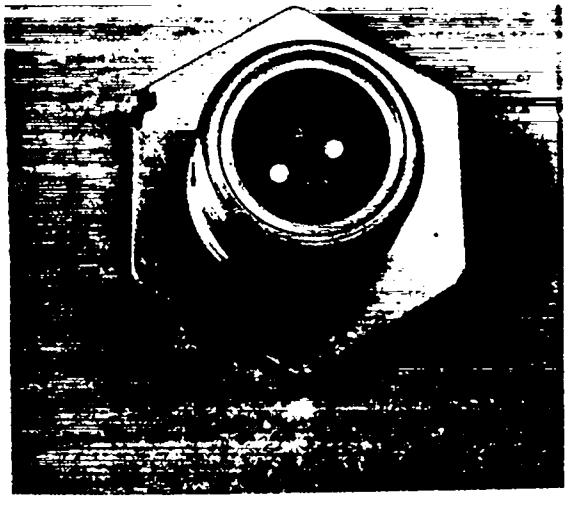

Fig. 3
The two 1.75-mm-long welded bridgewires are shown in the ER-322 header.

IV. THE NUMERICAL MODELS

A. EXPLO

Two computer codes were used in the modeling effort. The first code, which is used to describe the hot-wire ignition of explosives, is called EXPLO and was developed at the Los Alamos National Laboratory by Dwight L. Jaeger.[3] The following is the abstract from Ref. 3.

> The finite difference method is used to calculate temperature fields and times to initiation for explosive materials. The code is one-dimensional and is programmed for Cartesian, cylindrical, and spherical coordinates. Temperature-dependent properties, phase changes, and multiple heat source terms are allowed. Multiple source terms use Nth-order Arrhenius kinetics for each material component. Temperature, flux, convection or radiation boundary conditions may be employed. Internal convection is considered for materials that undergo a solid-liquid phase change. The Crank-Nicholson implicit solution method, which allows large time steps and short running time, is used.

A slight modification was made to EXPLO to allow for heat generation from an electric current passing through a resistance. The resistance is a function of both the nominal assembly resistance and the thermal coefficient of resistivity for the bridge being modeled. Because the one-dimensional code considers the bridge to be infinite in length, the initial resistance is input on a unit length basis. In this way, the same amount of heat will be generated in a length equal to that of the bridge being modeled.

With the exception of heat loss to the surrounding explosive, the heat transfer associated with a round bridgewire that is lying on a glass, plastic, or ceramic substrate and welded to electrodes at each end is a three-dimensional process. These heat losses are accounted for in the EXPLO code by creating a heat sink along the center of the wire. The coefficient of thermal conductivity and density of this heat sink are adjusted by considering the geometry and materials used in the hot-wire device being modeled, but the specific heat value, which is used for the internal heat sink, is the same as that of the substrate material.

In deriving the relationship for the adjusted coefficient of thermal conductivity, the temperatures of the substrate and electrodes are assumed to be

equal regardless of the wire temperature. In addition, the wire is considered to be isothermal over its length. These two assumptions produce a slightly larger coefficient of thermal conductivity, but the effect of this error will later be shown to be insignificant.

The relationship for the adjusted thermal conductivity coefficient in terms of geometry and material properties is

$$2\left[\frac{k_w A_w}{L/2}(T_w-T_o)\right] + \frac{k_s A_s}{R}(T_w-T_o) = \frac{k^* A}{R/8}(T_w-T_o), \qquad (1)$$

where

T_w = Wire temperature,
T_o = Electrode, substrate, and heat sink temperature,
k_w = Coefficient of thermal conductivity for the wire material,
k_s = Coefficient of thermal conductivity for the substrate material,
L = Length of wire being modeled,
R = Radius of wire,
A_w = Cross-sectional area of the wire $[\pi R^2]$,
A_s = Contact area with the substrate $[(\frac{\alpha}{2})(\pi)(2R)(L)$, where α is the angle of contact],
A = Surface area of internal heat sink $[2\pi(\frac{R}{4})L]$, and
k^* = Adjusted coefficient of thermal conductivity.

In Eq. (1), the radius of the internal heat sink was fixed at one-fourth the wire radius, and the distance through which the heat transfer was taking place in the heat sink was defined as half the heat sink radius. The heat transfer to the substrate was considered to occur through a distance equal to the wire radius. The effect on k^* of these distances of heat transfer is to cause it again to appear larger than had the full heat sink radius or the thickness of the substrate been used. This apparent increase of k^* by a factor of two or greater cancels out the effect of the isothermal assumptions made earlier.

The outcome of these and later assumptions is to limit the performance predicted by EXPLO. The true performance of the hot-wire ignition system that was modeled will lie between the bounds formed by considering this exaggerated heat loss and no heat loss at all.

By inserting the relationships for the areas and canceling like terms, the following relationship defines the adjusted coefficient of thermal conductivity used in the internal heat sink.

$$k^* = \frac{1}{4}\frac{\alpha}{\pi} k_s + \frac{k_w R^2}{L^2} \quad . \tag{2}$$

The first term results from substrate contact and the second from heat loss to the electrodes.

The density of the heat sink region is obtained from the substrate density and a scaling factor. The scaling factor is the ratio of a portion of the substrate volume to the volume of the internal heat sink. For identical lengths, this becomes a ratio of areas. The substrate area was fixed as a circle with a radius 7.5 times greater than the wire. This circular area is approximately the same as the half circle area shown in Fig. 4. This half circle has a radius ten times greater than the wire and, as the figure illustrates, represents a substantial portion of the substrate under the wire. As a result of the dimensions chosen, the adjusted density is 900 times the substrate density.

The use of a smaller scale factor would reduce the apparent mass of the heat sink, and the temperature of the heat sink would increase more rapidly.

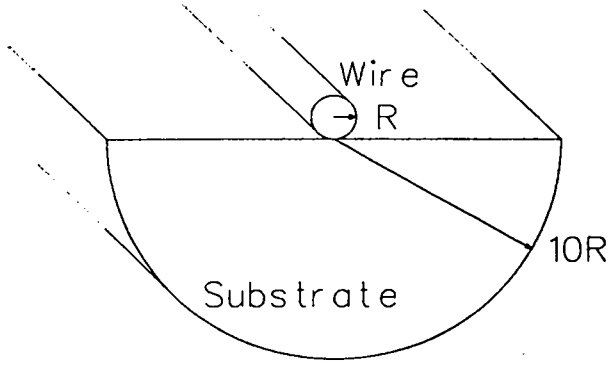

Fig. 4
The relative size of the wire to the portion of the substrate used to adjust the density of the heat sink is shown.

Because the amount of heat transferred to the heat sink is proportional to the temperature difference between the wire and the heat sink, the effect would be similar to a decrease in the coefficient of thermal conductivity.

With the exception of heat loss to the surrounding explosive, the heat transfer associated with a thin flat bridge that is deposited on a substrate is more easily handled by EXPLO. In this situation, the bridge is input as a horizontal layer between the substrate and explosive material layers. The thickness of each layer is the same as would be used in the actual electroexplosive device. A flat deposited bridge is generally very thin. Because the cross-sectional area of the bridge is small compared with the surface areas in contact with the explosive and substrate, heat losses through the ends and edges of the bridge are not compensated for.

B. ADINA

The second code, which was used to describe the shear of the flying plate, is called ADINA (Automatic Dynamic Incremental Nonlinear Analysis) and was developed at the Massachusetts Institute of Technology by Klaus-Jurgen Bathe.[4] ADINA uses the finite element method to perform static and dynamic displacement and stress analysis of solids and structures. ADINA allows both linear and nonlinear material descriptions, strains, and displacements.

The geometry of the flying plate and barrel is described in the analyses as a collection of two-dimensional axisymmetric solid elements. Figure 5 shows

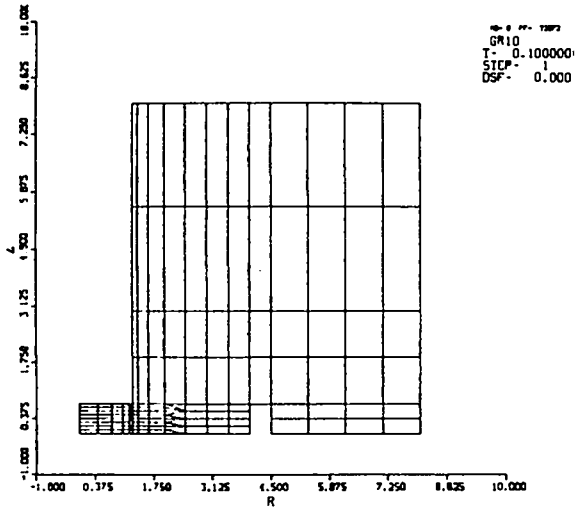

Fig. 5
Mesh diagram for a 0.75-mm-thick plate and a 2.5-mm-diam barrel combination.

a mesh diagram for a 0.75-mm-thick plate and 2.5-mm-diam barrel combination. Because the plate is a softer material than the barrel and the highest stresses are expected to occur in the plate, more elements are defined in the plate than in the barrel assembly. An even finer mesh is defined in the region of the plate under the edge of the barrel.

Initial calculations with linearly elastic material models indicated that the stress in the aluminum plate reached its ultimate strength before the steel barrel assembly reached yield strength at any point. Hence, the steel barrel was described accurately as being linearly elastic, whereas an elastic-plastic material model with a von Mises yield condition and kinematic hardening was used to describe the aluminum.

There is a problem, inherent in ADINA, with the aluminum material model. Although the material model recognizes the yield point and changes the material behavior accordingly, the failure that occurs when the material reaches its ultimate strength is not accounted for.

To overcome this problem, the flying plate was deemed to shear loose when the stress in an element node below the surface exceeded the ultimate strength of the material. This is a reasonable assumption because the stress in the remaining cross-sectional area would increase as the full load was carried by the reduced area. This increase in stress causes the next node in line to exceed the ultimate strength and reduce the area even further. In a time span much smaller than the increment of time between ADINA calculations, this cascade of failing nodes would cause the plate to shear. There was little difference in the results if the von Mises or first principal stress was used.

In the analysis, pressure is applied over an area corresponding to the surface of the explosive. Any pressure-time profile can be input as a series of short linear segments.

V. EXPLO RESULTS

A. Effect of Heat Losses

The results obtained from EXPLO that compare the effect of the various heat losses from a 0.051-mm-diam wire in an ER-322 device are shown in Fig. 6. The three curves represent no heat loss from the wire (other than to the explosive), heat loss through the ends of the wire to the electrodes, and heat loss through the ends of the wire to the electrodes and to the substrate

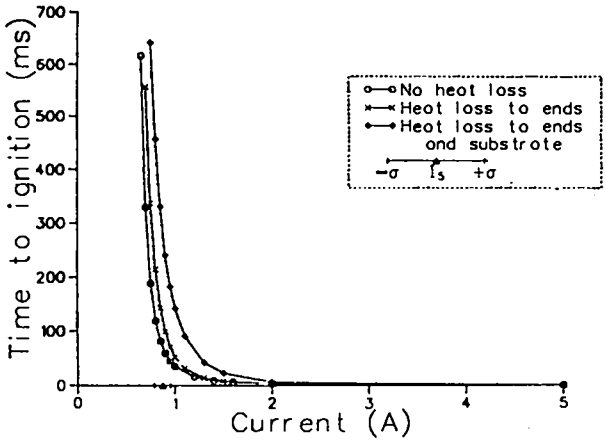

Fig. 6
EXPLO-calculated time to ignition for three modes of heat loss. The experimentally determined threshold is shown on the current axis.

through contact along a wire length of 1.76 mm. The adjusted coefficient of thermal conductivity to the heat sink is ten times greater when contact with the substrate is included.

The triangle on the current axis of Fig. 6 indicates the experimentally determined threshold firing current. The two vertical marks to each side of the triangle are placed at one standard deviation above and below the threshold. EXPLO indicates a substantial increase in the time to ignition in the threshold region. At three standard deviations below the threshold current, only one in a thousand devices should function; the increasing vertical slopes of the two curves that include heat losses imply that these devices would not function three standard deviations below the experimentally determined threshold point.

At high current levels, the calculated time to ignition is the same for each of the curves. The bridge is being heated so rapidly that there is no appreciable heat transfer before ignition of the explosive occurs.

The mashing of the wire during welding would reduce the cross-sectional area through which heat could be transferred to the electrode. The maximum effect of the reduction in area would be to shift the threshold level by the difference in the two curves, shown in Fig. 6, representing no heat loss and heat loss through the ends of the wire. Intermittent contact of the wire with the substrate would cause a similar shift in performance, which is bounded by the curve representing complete contact and the curve with losses only through the wire ends.

B. Function Time Comparisons

The function times that were experimentally measured at -54°C are plotted in Fig. 7. Also plotted are the calculated times to ignition for the three heat loss conditions. It is evident that the inclusion of heat loss to the substrate produces error.

This result prompted a review of bridged headers identical to those used in the function time measurements. Welding the wire to the electrodes caused the wire to arch slightly. This arching prevented the bridgewire from making contact with the substrate at any point along the wire length. As a result of this, heat transfer to the substrate was not considered in any of the subsequent calculations.

The differences in function time are plotted in Fig. 8. The graph includes a line that represents the location of points where the difference between two calculated times to ignition is equal to the difference between two measured function times. If the only variation in the measured function time is due to the time to ignition changing with the firing current, the closeness of the calculated difference to the equality line is an indication of accuracy. The

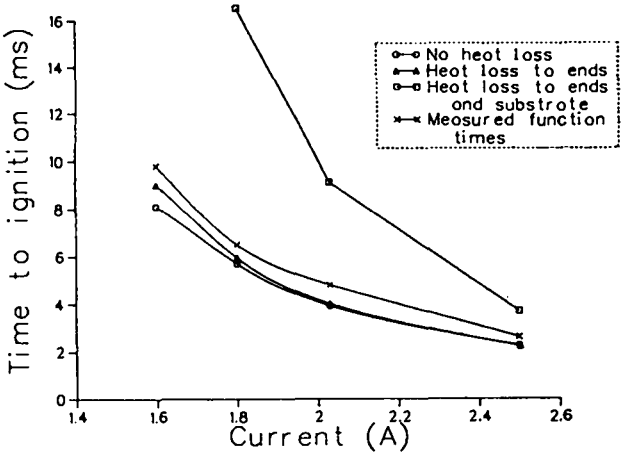

Fig. 7
EXPLO-calculated time to ignition for three modes of heat loss at -54°C. The experimentally determined function times are also plotted.

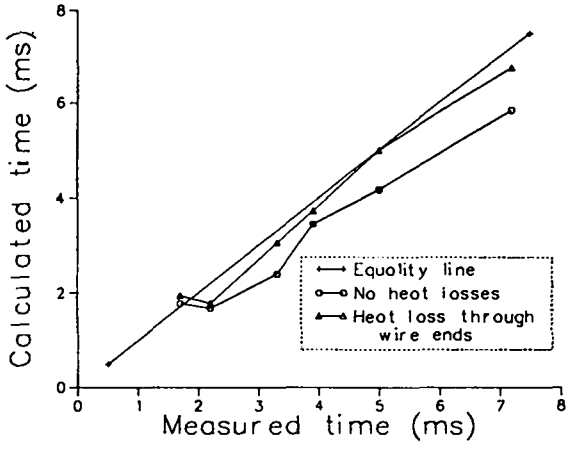

Fig. 8
The differences between calculated ignition times are plotted against the corresponding differences in measured function times.

curve produced from calculations that include the heat loss through the ends of the wire seems to show excellent agreement.

C. Firing Current Threshold

Figures 9 through 14 show the time-to-ignition vs current curves for 0.028-, 0.033-, 0.035-, 0.039-, 0.046-, and 0.051-mm-diam NiCr wires respectively. The triangle on the current axis of each figure indicates the experimentally determined threshold firing current, and the two vertical marks to each side of the triangle are placed at one standard deviation above and below the threshold.

One observation can be made concerning these six figures that was not made with respect to Fig. 6. Because each of the graphs is to the same scale, the measured threshold point on each curve seems to correspond with the same location on the bend of the curve. This implies that the experimentally determined threshold corresponds to some slope of the calculated time-to-ignition vs current curve.

The negative of the slope of the time-to-ignition curve for the 0.035-mm-diam wire shown in Fig. 11 is plotted in Fig. 15. This graph is representative

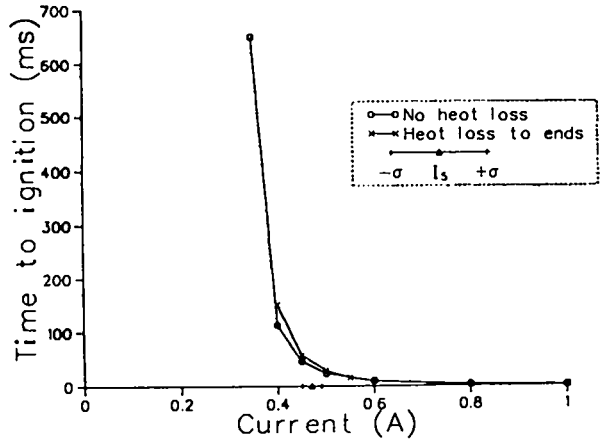

Fig. 9
EXPLO-calculated time to ignition for a 0.028-mm-diam NiCr bridgewire. The experimentally determined threshold is shown on the current axis.

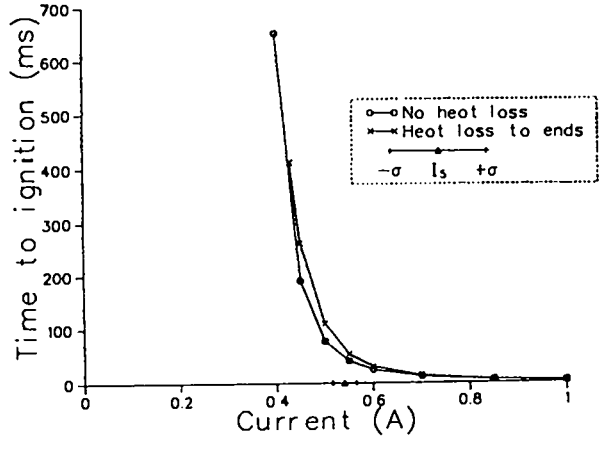

Fig. 10
EXPLO-calculated time to ignition for a 0.033-mm-diam NiCr bridgewire. The experimentally determined threshold is shown on the current axis.

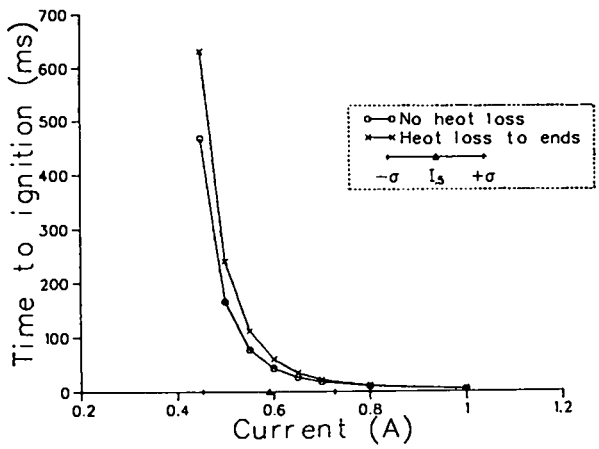

Fig. 11
EXPLO-calculated time to ignition for a 0.035-mm-diam NiCr bridgewire. The experimentally determined threshold is shown on the current axis.

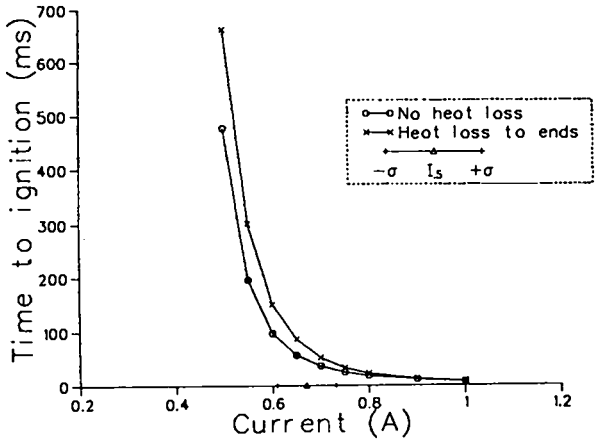

Fig. 12
EXPLO-calculated time to ignition for a 0.039-mm-diam NiCr bridgewire. The experimentally determined threshold is shown on the current axis.

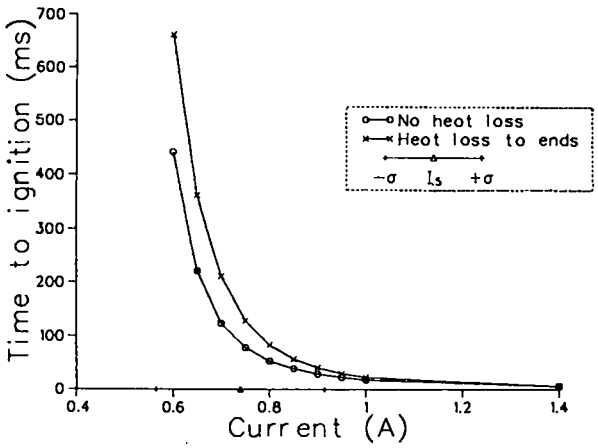

Fig. 13
EXPLO-calculated time to ignition for a 0.046-mm-diam NiCr bridgwire. The experimentally determined threshold is shown on the current axis.

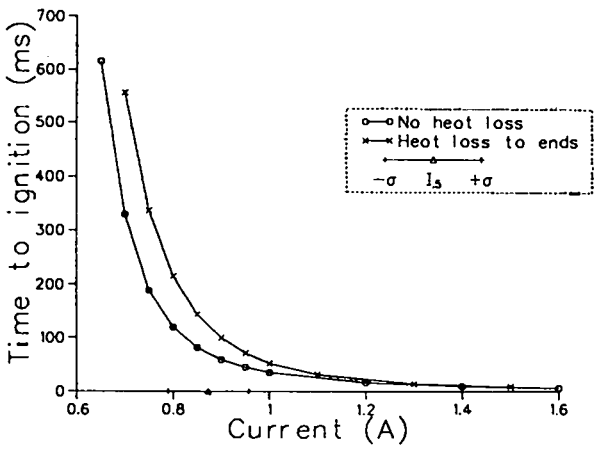

Fig. 14
EXPLO-calculated time to ignition for a 0.051-mm-diam NiCr bridgewire. The experimentally determined threshold is shown on the current axis.

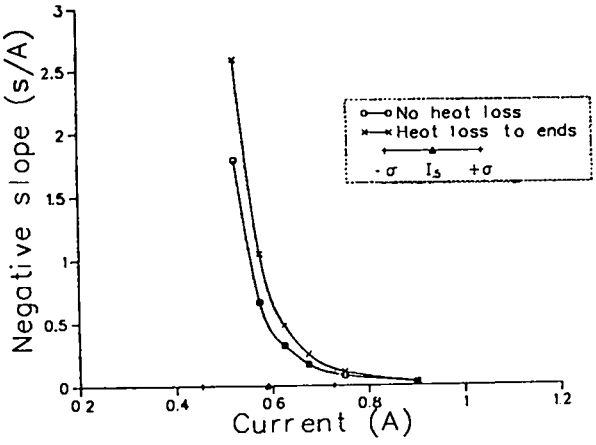

Fig. 15
Slope of time-to-ignition curve for a 0.035-mm-diam NiCr bridgewire. The experimentally determined threshold is shown on the current axis.

of the plots obtained for each wire diameter. The current threshold and standard deviation limits are again shown by a triangle and vertical marks on the current axis.

Figure 15 shows that the threshold corresponds to a slope of about 0.5 for the calculations without heat loss and 0.75 for the calculations that include heat transfer through the ends of the wire. The slope at a current level one standard deviation below the threshold is essentially infinite because of the magnitude of the standard deviation and the steepness of the curve.

The negative of the slope at threshold and at one standard deviation above and below the threshold is shown for each of the six wire diameters in Figs. 16 and 17. The points in Fig. 16 were obtained from calculations that did not include heat losses through the ends of the wire. In this figure, the threshold levels seem to correspond to a slope of about 0.5. The relatively large deviation from 0.5 by the 0.046-mm-diam wire is not considered significant because of the large standard deviation associated with the experimental threshold determined for this wire diameter.

The points in Fig. 17 were obtained from calculations that included the heat losses through the ends of the wire to the electrodes. The threshold levels seem to correspond to slopes of about 0.7 or 0.8. As stated before, the deviation associated with the 0.046-mm-diam wire is not significant. In fact, more variability would be expected in Fig. 17 because of the reduction in cross-sectional area during welding.

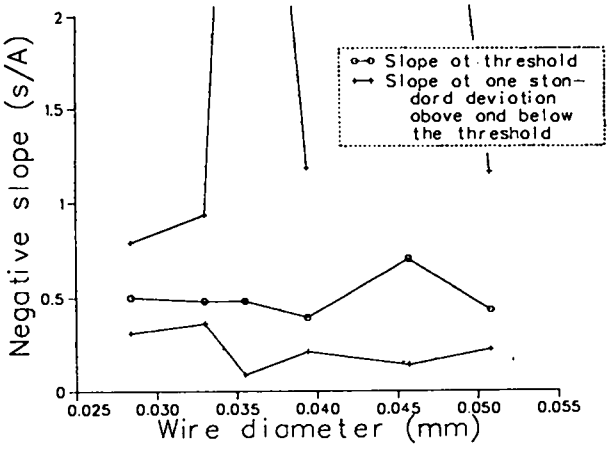

Fig. 16
The slope of the calculated time-to-ignition vs current curve at the experimentally determined threshold current level is plotted, and no wire heat loss is included.

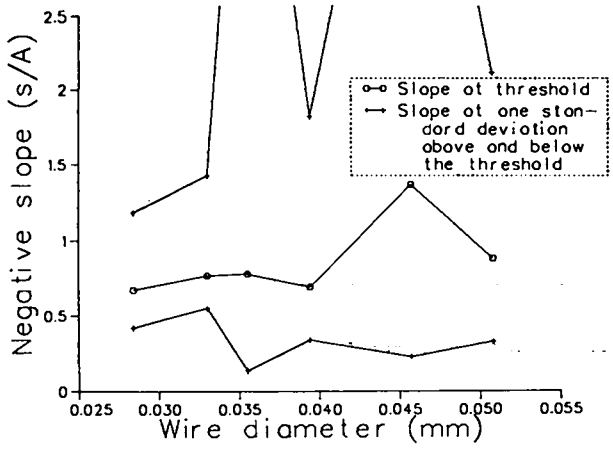

Fig. 17
The slope of the calculated time-to-ignition vs current curve at the experimentally determined threshold current level is plotted, and wire end heat loss is included.

D. Wire Length

Although no experimental data were available, EXPLO was used to predict the effect of increasing the wire length from 1.76 to 2.26 mm in the ER-322. This 0.5-mm increase in length could easily be obtained as a manufacturing variable by welding the wire to a slightly different position on each of the 1.0-mm-diam electrodes.

The time-to-ignition vs function curves are shown in Fig. 18 for the two wire lengths. The slopes of these two curves are plotted in Fig. 19, and a line indicating a threshold slope of 0.75 is also plotted.

The 0.5-mm increase in wire length only changed the predicted threshold current from 0.87 to 0.89 A or by about 2%. However, the increase in length changed the resistance from 0.88 to 1.12 ohms or by 22%. This increased the power from 0.67 to 0.90 W or by 25%.

E. Wire Material

The last EXPLO calculation that will be reported is a change of the wire material in the ER-322 from Tophet C to gold. Again no experimental data are available with which to compare the predictions.

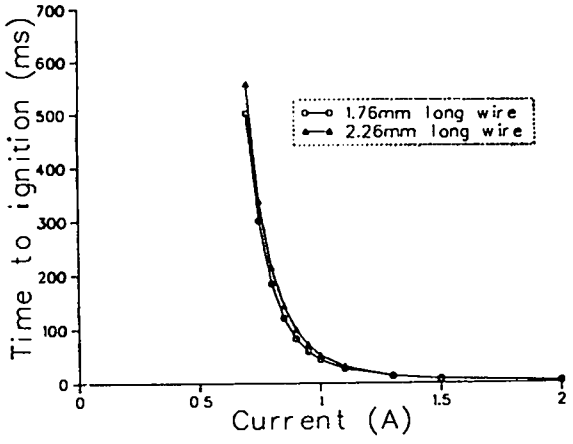

Fig. 18
EXPLO-calculated time to ignition for wire lengths of 1.76 and 2.26 mm. The two plots represent a wire diameter of 0.051 mm with heat loss through the ends of the wire.

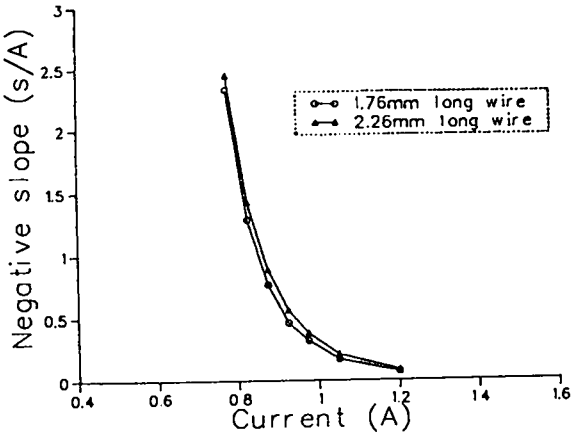

Fig. 19
Slope of the time-to-ignition curves for wire lengths of 1.76 and 2.26 mm. The dotted line indicates the region of the curves where the slope is 0.75 s/A.

The time-to-ignition curves for 1.76-mm-long and 0.051-mm-diam wires of the two materials are shown in Fig. 20. To achieve ignition in a time period of 330 ms, the Tophet C and gold bridgewires require currents of 0.75 and 3.5 amps, respectively. However, because the resistance of the gold wire is only 2% of the Tophet C wire, considerably less power is required to ignite the HMX explosive with a gold wire.

VI. ADINA RESULTS

In analyzing the shear of the flying plate with ADINA, calculations were first made to observe the effect of the rate at which pressure was applied to the plate on the pressure level at which the plate was deemed to have sheared. Next, a number of calculations were made to compare combinations of barrel diameter and plate thickness. A regression analysis was performed with the results of these ADINA computations to derive a relationship for the pressure level at which the aluminum flying plate shears as a function of the barrel diameter and plate thickness. The loads at which the plate sheared were also used to predict flying plate velocities, and these velocities were compared with experimentally inferred velocities.

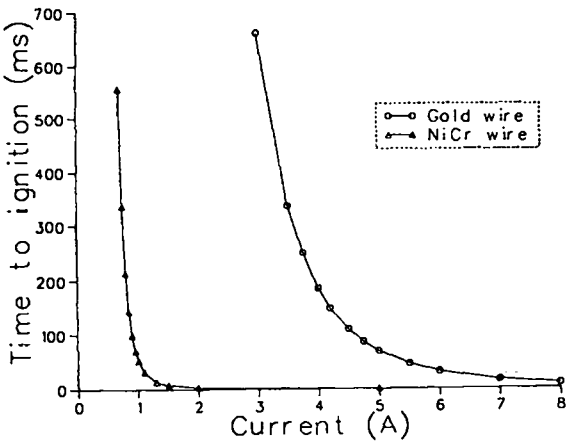

Fig. 20
EXPLO-calculated time to ignition for wire materials of gold and NiCr. The two plots represent a wire diameter of 0.051 mm with heat loss through the ends of the wire.

A. Rate of Pressure Loading

The rate at which pressure is applied to the plate is not known. In all of the ADINA calculations, the pressure was assumed to increase linearly with time. The initial calculations with ADINA, where linearly elastic material models were used, indicated that the stresses in the aluminum plate reached the ultimate material strength at a pressure load of about 200 MPa.

At electric current levels of 1.6 and 2.0 A, respectively, function times of 9.8 and 4.8 ms were measured and times to ignition of 9.0 and 4.0 ms were calculated. In both cases, the difference between the function time and ignition time was 0.8 ms. Because the flying plate would take about 14 μs to travel the 7.0 mm to close the switch, the 0.8 ms is, for the most part, the time from start of pressure to plate shear. To reach a pressure load of 200 MPa in 0.8 ms, a pressure rate of 250 MPa/ms is needed.

The acoustic velocity for aluminum with a modulus of 69 000 MPa and a density of 2.71 g/cm^3 is 5000 m/s. At this speed, a shock wave would take 0.15 μs to traverse a 0.75-mm-thick plate. Because this time is so short compared with the pressure loading rate, the actual rate at which pressure is applied to the plate surface should not affect the load at which the flying plate shears loose.

To verify that ADINA would exhibit this effect, two analyses were executed with pressure rates of 250 MPa/ms and 2500 MPa/ms. For these calculations, a barrel diameter of 2.5 mm and a plate thickness of 1.0 mm were used. Fig. 21 shows the von Mises stress contours in the region of the plate after 0.6 ms

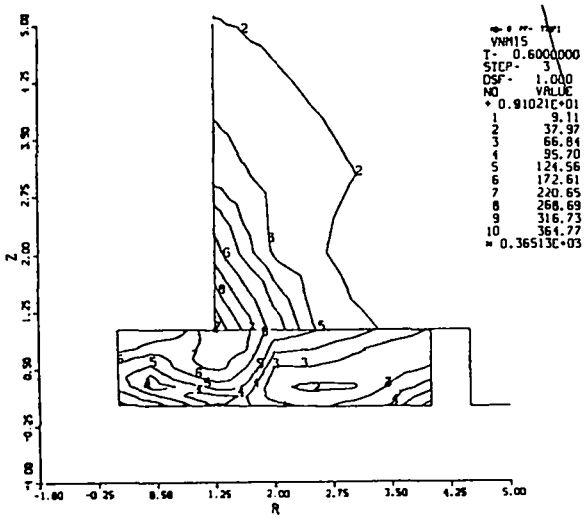

Fig. 21
Von Mises stress contours in a 1.0-mm-thick aluminum plate at a pressure of 150 MPa. The pressure application rate is 250 MPa/ms.

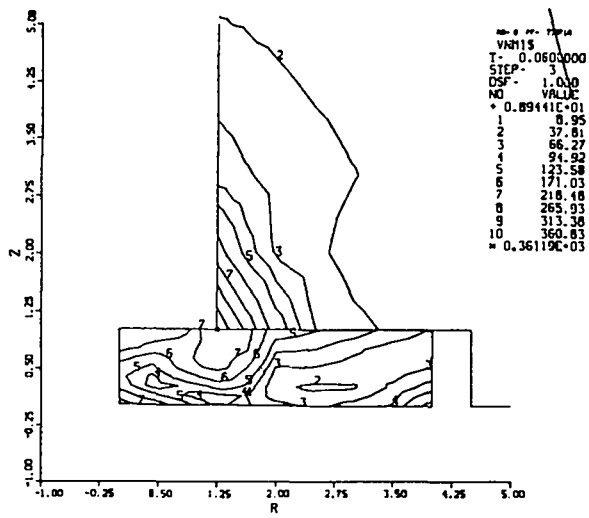

Fig. 22
Von Mises stress contours in a 1.0-mm-thick aluminum plate at a pressure of 150 MPa. The pressure application rate is 2500 MPa/ms.

when the load is 150 MPa. Figure 22 shows the same contours after 0.06 ms when the load is also 150 MPa because of the 2500 MPa/ms loading rate. Contour #7 is the highest stress in the plate, and the magnitude of this stress differs by only 1% when the pressure load rate is increased by a factor of 10.

The results from these two analyses imply that the model will give a consistent indication of the stress in the plate even though the actual rate at which pressure is applied to the plate surface is unknown. The rate that pressure is applied is slow enough to eliminate inertial effects, and the ADINA material model does not take into account the effects of strain rate.

B. Effect of Diameter and Thickness

To evaluate the effect of barrel diameter and plate thickness on the pressure level at shear, nine ADINA calculations were executed. Barrel diameters of 1.25, 2.5, and 5.0 mm were combined with aluminum plate thicknesses of 0.5, 0.75, and 1.0 mm.

As a representative example, the results obtained from ADINA for a barrel diameter of 2.5 mm and a plate thickness of 0.75 mm are presented in Figs. 23 through 32. Figures 23 through 26 show the von Mises stress contours in the region of the plate up to a load of 200 MPa. At 200 MPa in Fig. 26, contour #7

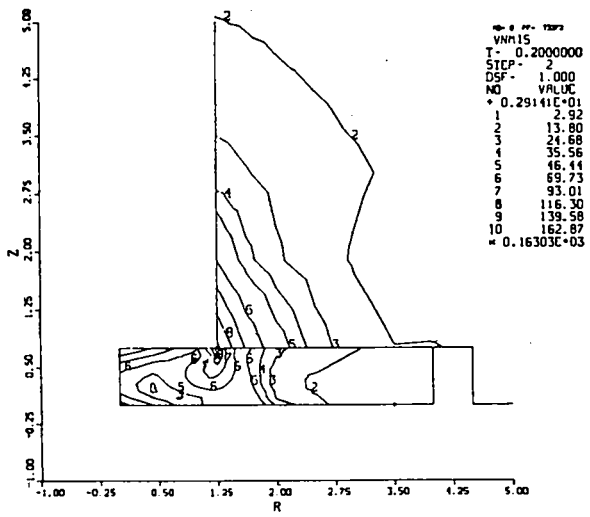

Fig. 23
Von Mises stress contours for a 0.75-mm-thick plate and a 2.5-mm-diam barrel. The pressure is 50 MPa.

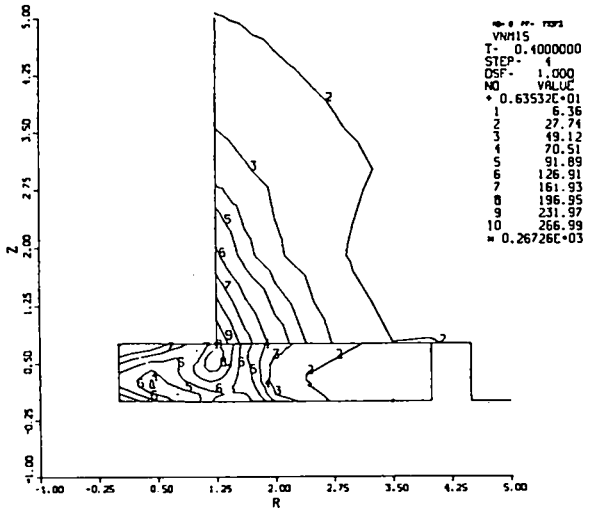

Fig. 24
Von Mises stress contours for a 0.75-mm-thick plate and a 2.5-mm-diam barrel. The pressure is 100 MPa.

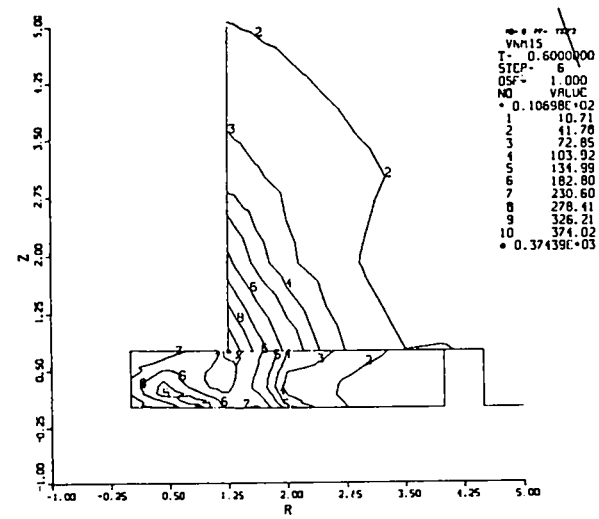

Fig. 25
Von Mises stress contours for a 0.75-mm-thick plate and a 2.5-mm-diam barrel. The pressure is 150 MPa.

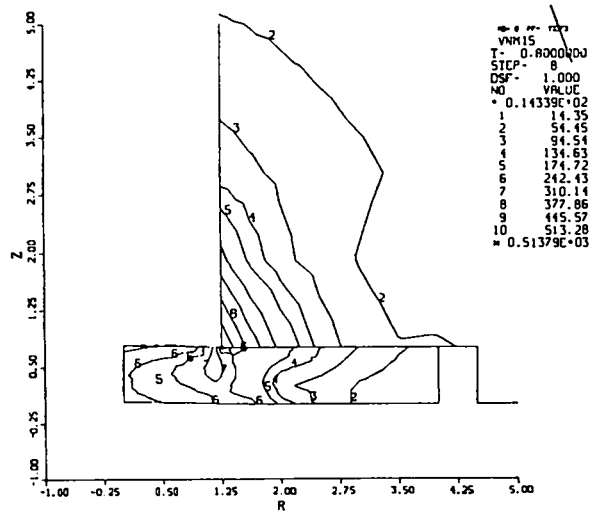

Fig. 26
Von Mises stress contours for a 0.75-mm-thick plate and a 2.5-mm-diam barrel. The pressure is 200 MPa.

has exceeded the ultimate material strength of 289 MPa for the aluminum. Figures 27 through 30 show the contours for the first principal stress.

Figures 31 and 32 show the von Mises and first principal stress, respectively, as a function of time for four nodes. These four nodes are adjacently located on a line 0.09 mm below, and parallel to, the upper surface of the plate. The third of these nodes is located directly below the edge of the barrel. In Fig. 31, the second node reaches 289 MPa at about 0.68 ms, and in Fig. 32, the second node reaches 289 MPa at about 0.71 ms. At a pressure rate of 250 MPa/ms, these two times correspond to load levels of 170 and 177 MPa, respectively.

The results obtained from Fig. 31 and similar graphs for the other eight barrel diameter and plate thickness combinations are tabulated in Table I. Also given are the results from a two-variable linear regression analysis.[5]

The following relationship was obtained for the pressure level at which the flying plate was deemed to shear loose as a function of the barrel diameter

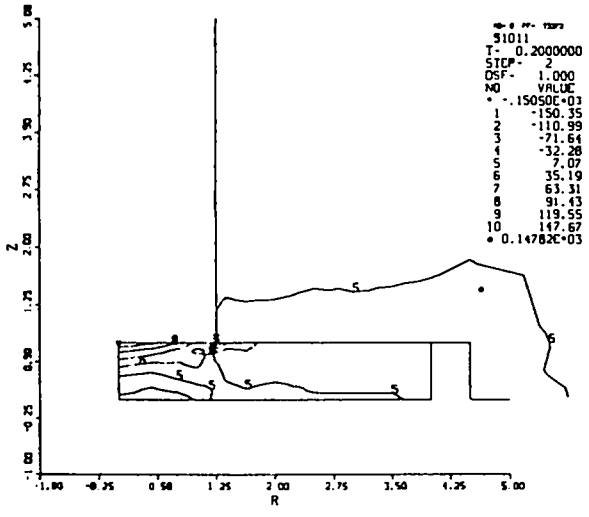

Fig. 27
First principal stress contours for a 0.75-mm-thick plate and a 2.5-mm-diam barrel. The pressure is 50 MPa.

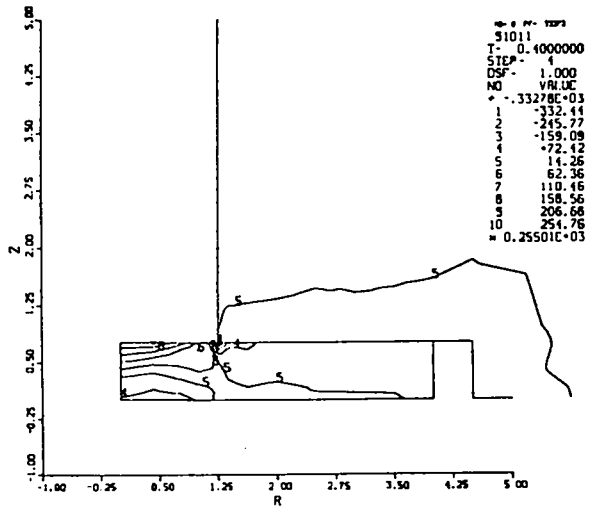

Fig. 28
First principal stress contours for a 0.75-mm-thick plate and a 2.5-mm-diam barrel. The pressure is 100 MPa.

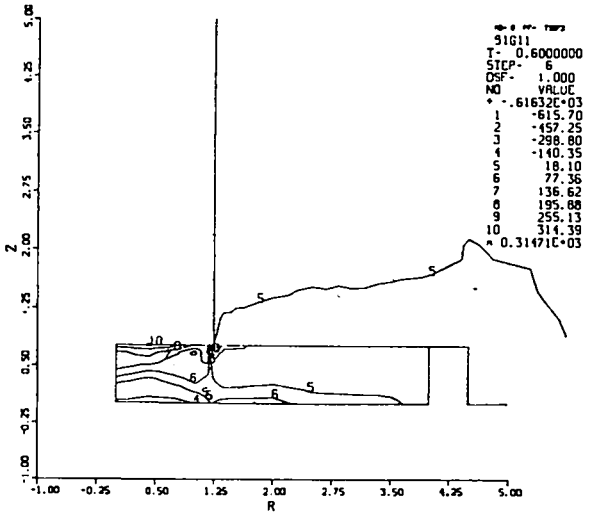

Fig. 29
First principal stress contours for a 0.75-mm-thick plate and a 2.5-mm-diam barrel. The pressure is 150 MPa.

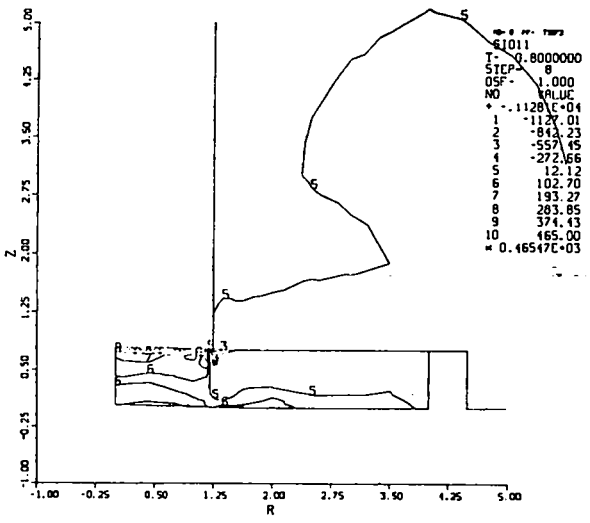

Fig. 30
First principal stress contours for a 0.75-mm-thick plate and a 2.5-mm-diam barrel. The pressure is 200 MPa.

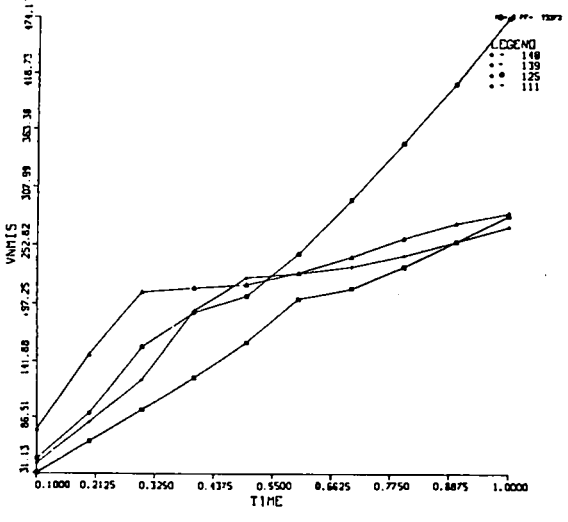

Fig. 31
Von Mises stress contours in four nodes located below the surface of the plate and near the edge of the barrel.

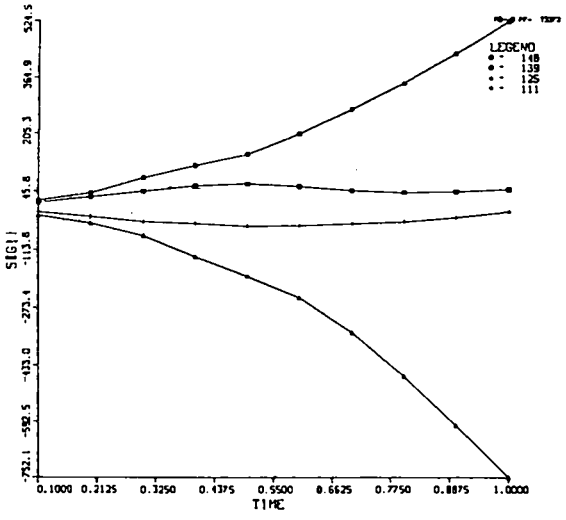

Fig. 32
First principal stress contours in four nodes located below the surface of the plate and near the edge of the barrel.

TABLE I

ADINA COMPUTED PRESSURE AT SHEAR AND
REGRESSION ANALYSIS RESULTS

Pressure at Shear

Plate Thickness (mm)	Barrel Diameter (mm)	ADINA (MPa)	Regression (MPa)	Difference (%)
1.0	5.0	102	101	1
1.0	2.5	200	217	8
1.0	1.25	281	276	2
0.75	5.0	75	67	10
0.75	2.5	170	183	7
0.75	1.25	256	241	6
0.5	5.0	37	32	13
0.5	2.5	120	148	19
0.5	1.25	219	207	5

and aluminum plate thickness.

$$P = 194.5 + 138.0t - 46.5d\,, \tag{3}$$

where

P = Pressure load in MPa,

t = Aluminum plate thickness in mm, and

d = barrel diameter in mm.

Table I lists the pressure level at failure as calculated by Eq. (3) and an indication of the deviation from the ADINA calculated failure level. The average deviation is about 8%.

C. Flying Plate Velocities

The pressure load when the flying plate shears loose can be used to derive a velocity with two important assumptions. The first of these assumptions deals with the pressure that pushes the plate.

The pressure on the plate could decrease, remain constant, or increase as the plate is pushed down the barrel. A decreasing pressure would occur if the reacting material in the electroexplosive device ceased to generate gas when

the plate sheared or the rate of gas generation is insufficient to offset the expanding volume. The pressure on the plate would increase only if the gas generation rate is more than sufficient to offset the volumetric expansion. Lacking any better data, the gas pressure was assumed to stay constant at a level equal to the pressure at which shear occurs.

The second assumption deals with the movement of the flying plate along the surface of the barrel. Contact between the plate and the barrel surfaces would produce friction and retard the plate movement. However, measurement of the diameters of several flying plates that were recovered indicated that the flying plate is slightly smaller than the barrel. The fact that the second node in Figs. 31 and 32 experienced the highest stress, supports the idea that the flyer is smaller because this node is 0.08 mm away from the edge of the barrel. Lacking any better idea, the movement was assumed to be frictionless because of gas release around the edge of the flying plate that would tend to center the plate in the barrel and prevent edge contact.

The pressure over the area of the flying plate produces a force. The thickness and diameter of the flying plate determine a mass. The force and mass determine an acceleration from which a velocity can be calculated after 7.0 mm of travel down the barrel. These calculated velocities are given in Table II.

TABLE II

COMPUTED VELOCITY FOR CONSTANT PRESSURE

Plate Thickness (mm)	Barrel Diameter (mm)	Pressure at Shear (MPa)	Velocity at 7.0 mm (mm/μs)
1.0	5.0	102	.7
1.0	2.5	200	1.0
1.0	1.25	281	1.2
0.75	5.0	75	.7
0.75	2.5	170	1.1
0.75	1.25	256	1.3
0.5	5.0	37	.6
0.5	2.5	120	1.1
0.5	1.25	219	1.5

Although the calculated velocities may be substantially in error, such an analysis is useful for determining what changes in plate thickness and barrel diameter are needed to get a desired increase in velocity.

The estimated velocity for the 0.75-mm-thick by 2.5-mm-diam flying plate is 1.1 mm/μs. This velocity is sufficient to detonate PETN explosive but would not detonate HNS explosive, which is consistent with the experimental observations.

D. Flying Plate Integrity

Another useful observation was made in evaluating the stresses in the aluminum plate before shear occurs. Figure 33 shows the von Mises stress contours in a 0.75-mm aluminum plate in combination with a 5.0-mm-diam barrel at a pressure load of 75 MPa. This figure corresponds to the load at which the flying plate was deemed to shear loose. Even though the stresses have just reached the ultimate strength of the material near the edge of the barrel, stress contour #8 near the center of the plate shows that the plate has already failed. This mode of failure would not send a flying plate down the barrel.

The same observation was made with the 0.5-mm-thick by 5.0-mm-diam combination. The 0.5-mm-thick by 2.5-mm-diam combination appeared to be marginal. This implies that there is a minimum ratio of plate thickness to barrel diameter that must be maintained, and use of ADINA also provides a means of examining the flying-plate integrity.

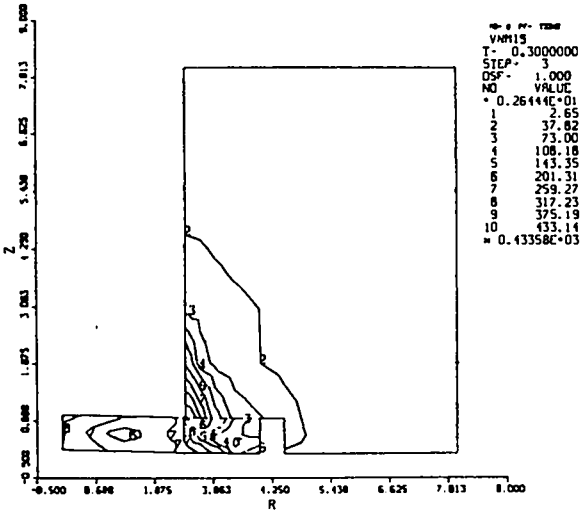

Fig. 33
Von Mises stress contours in a 0.75-mm-thick aluminum plate at a pressure of 75 MPa. The barrel diameter is 5.0 mm.

VII. SUMMARY AND CONCLUSIONS

The two existing computer codes that were used to model the igniting of an explosive by a hot wire and the shear of a flying plate produced excellent agreement with experimental data obtained from the ER-322 detonator. In the case of the code EXPLO, calculated times to ignition of HMX explosive were in harmony with function times that were experimentally determined. The agreement was so close that EXPLO predictions indicating that the bridgewires in the ER-322 detonators tested were not in contact with the substrate were later verified by inspection of welded bridgewires before they were covered with HMX. This result demonstrates that EXPLO can be used to evaluate the effect of manufacturing variations on performance.

EXPLO was also shown to be useful in predicting the current threshold. For six diameters of bridgewire, the same slope in each of the curves representing the calculated time to ignition as a function of current corresponded to the experimentally determined threshold. Although the value of the slope at threshold changed significantly when heat transfer to the electrodes was considered, the slope value was still consistent regardless of wire diameter. This result is evidence that EXPLO can be used as a design aid to predict the firing level of a hot-wire device, and a conservative estimate of the no-fire level is obtained when heat transfer to the electrodes is ignored.

The use of the code ADINA in analyzing the shear of a flying plate produces several useful results. The code is used to generate stress contours in the plate, and these contours can be used to evaluate the integrity of the flying plate and the pressure when the plate shears. The pressure that causes shear can also be used to infer a flying plate velocity. Experimental data indicate that the inferred velocity of 1.1 mm/μs for the ER-322 flying-plate detonator is approximately correct.

The employment of ADINA as a design aid allows the barrel diameter, plate thickness, and plate material to be varied so that the optimum combination of flying plate velocity and mass can be obtained without experimentation. By determining the pressure that causes the plate to shear, ADINA also indicates the strength required for the detonator body.

REFERENCES

1. B. M. Dobratz, Ed., "Properties of Chemical Explosives and Explosive Simulants," Lawrence Livermore Laboratory report UCRL-51319 (1972).

2. R. H. Dinegar and D. T. Varley, "All-Secondary Explosive Hot-Wire Devices," Los Alamos Scientific Laboratory report LA-7897-MS (October 1979).

3. D. L. Jaeger, "EXPLO: Explosives Thermal Analysis Computer Code," Los Alamos Scientific Laboratory report LA-6949-MS (January 1978) [Revision in progress].

4. K. J. Bathe, "ADINA: A Finite Element Program for Automatic Dynamic Incremental Nonlinear Analysis," Massachusetts Institute of Technology report 82448-1 (September 1975).

5. K. A. Brownlee, Statistical Theory and Methodology in Science and Engineering (John Wiley & Sons, New York, 1965).

Printed in the United States of America
Available from
National Technical Information Service
US Department of Commerce
5285 Port Royal Road
Springfield, VA 22161

Microfiche $3.50 (A01)

Page Range	Domestic Price	NTIS Price Code	Page Range	Domestic Price	NTIS Price Code	Page Range	Domestic Price	NTIS Price Code	Page Range	Domestic Price	NTIS Price Code
001-025	$ 5.00	A02	151-175	$11.00	A08	301-325	$17.00	A14	451-475	$23.00	A20
026-050	6.00	A03	176-200	12.00	A09	326-350	18.00	A15	476-500	24.00	A21
051-075	7.00	A04	201-225	13.00	A10	351-375	19.00	A16	501-525	25.00	A22
076-100	8.00	A05	226-250	14.00	A11	376-400	20.00	A17	526-550	26.00	A23
101-125	9.00	A06	251-275	15.00	A12	401-425	21.00	A18	551-575	27.00	A24
126-150	10.00	A07	276-300	16.00	A13	426-450	22.00	A19	576-600	28.00	A25
									601-up	†	A99

†Add $1.00 for each additional 25-page increment or portion thereof from 601 pages up.